Synchronization of geophysically-driven oscillators with short-range interaction

Cong Wei, *Student Member, IEEE,* and Herbert G. Tanner, *Senior Member, IEEE*

***Abstract*—This paper presents a method to synchronize a network of spatially distributed nonlinear oscillators that can only interact with each other intermittently and at very close proximity. This problem arises in applications where semi-passive sensors drift along patterns of ambient geophysical flows that bring them close periodically, and have to establish periodic rendezvous in order to efficiently exchange information or be retrieved. The problem is challenging because cooperative control action can only be applied over the short time window that agents are in rendezvous, and in over the whole network different groups, some of which share members, meet asynchronously. In cases such as these, the ambient geophysical dynamics that drive the motion of the agents need to be directly incorporated into control design. The paper presents a decentralized, intermittently activated, pairwise interacting control law for the agents, which under reasonable conditions on overall network connectivity, brings the whole system into a steady state where all agents synchronize their periodic rendezvous around configurations determined by the surrounding geophysical field.**

***Index Terms*—Nonlinear oscillators, synchronization, coordination, pattern formation, multi-agent systems.**

I. Introduction

THIS paper addresses the problem of synchronizing a spatially distributed network of intermittently interacting semi-passive mobile sensors, which are drifting along a dominant flow field, with limited actuation capability that only allows them to briefly accelerate along their own periodic orbits. The motivating application problem is the deployment of swarms of marine robotic sensor drifters over very large areas of ocean, where they can leverage natural ocean circulation [1]–[6] to collect data [7], [8]. Here, it is assumed that the sensors can intermittently communicate and interact with each other only over very short (compared to the scale of their motion paths) distances, specifically at those instances where their trajectories are proximal. Synchronization of this intermittent spatially distributed network may be desirable in cases where data should be shared for robustness purposes, increase of area coverage and observation persistence [7], [9], [10], energy savings and endurance improvement [11]–[14] from the reduction in satellite communications, or when the sensors are to be picked up at the end of their mission. Similar application scenarios can be encountered in deployments of heterogeneous mobile robot teams [15], or coordinated groups of unmanned marine vehicles, on the surface or underwater [16], e.g. in cooperative mine countermeasure [17] or search and recovery missions [7], [8].

In this paper the problem is formulated in the context of networks of robotic drifters who need to rendezvous on a shared two-dimensional workspace [8], but the control objective is to achieve synchronized periodic rendezvous (cf. [18]) under the constraint of local interaction (cf. [19]). Here, synchronization through periodic rendezvous is understood as a steady state in which robotic drifters moving along neighboring current circulations periodically and intermittently come in close proximity. One distinguishing characteristic of the problem formulation of this paper is that agent motion is driven (primarily) by an ambient vector field, modeling a geophysical flow pattern that is dominant in the workspace in which the agents are deployed; e.g., the robotic drifters will not spend their precious power reserves to fight the current that drives them. For the purposes of this analysis, it is assumed that this ambient flow takes the form of a grid of gyres that give rise to Lagrangian coherent structures (LCS) [20]. In fact, it has been suggested that such ocean circulation patterns could be leveraged to improve the endurance of environmental monitoring, weather, and climate forecasting sensors [20]–[22].

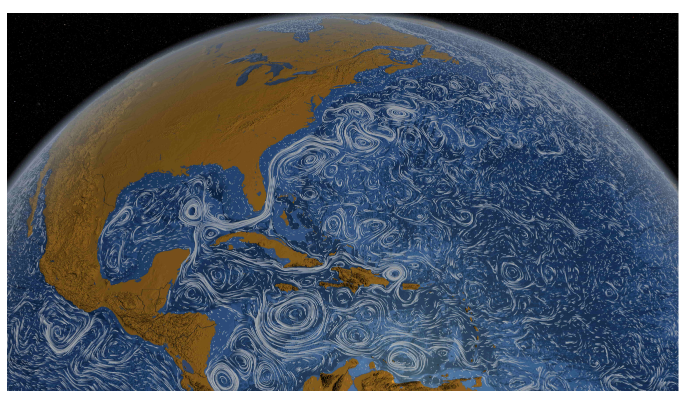

Fig. 1: Snapshot (August 2005) of visualization of ocean surface currents for June 2005 through December 2007 generated using NASA/JPL's ECCO2 ocean model. Link: https://svs.gsfc.nasa.gov/3827

Tanner and Wei are with the Department of Mechanical Engineering, University of Delaware, Newark, DE 19716 USA. e-mail: {weicong,btanner}@udel.edu.

Special thanks to M. Ani Hsieh, Dhanushka Kularatne and Xi Yu providing access to facilities, material, equipment, and assistance in experimental work associated with implementation aspects of early control design prototypes.

This work is supported by ONR through grant no N000141712690.

Earlier approaches to this problem [23], [24] examined conditions under which drifters in neighboring gyres can move within rendezvous range of one another by leveraging this ambient flow dynamics. It has been demonstrated that this can be achieved even in the presence of stochastic disturbances [25]. In these early synchronization control designs [23], the flow-induced drifter dynamics was modeled in the form of a harmonic oscillator. The oscillators' phases, representing robot positions, achieve synchronization through a (linear) time-optimal control law designed to maximize the brief time interval in which they remain in rendezvous. In principle, the rendezvous conditions can be extended to more realistic (albeit still simplistic) nonlinear periodic circulation models; however, the presence of nonlinearities and the desire to handle uncertainty motivate the use of sliding mode control laws for achieving and maintaining synchronization [26]. Time-optimality and maximization of the robotic drifter rendezvous time can be recovered in this nonlinear setting through a nonlinear transformation, under the assumption that the robots' communication range is negligible compared to the spatial scale of their orbit [27].

There is a body of work on the problem of synchronization of coupled oscillators which appears in a diverse collection of literature related to physics, neurology, and chemistry [28]–[31]. In this context, synchronization is understood as the state in which the the phase difference between neighboring oscillators is locked to zero [28], [32]. However, all this work is premised on neighboring oscillators interacting continuously with each other. Multi-agent coordination with intermittent or periodic connectivity or coupling has been received some attention [19], [30], [33]–[35], motivated by application cases where communication can occur over very short range or where obstacles disturb line-of-sight communication links [36]. Intermittent interaction has also been proposed as a means of alleviating local storage limitations and facilitating local plan execution [35], [37]. The same concept, through the form of fixed-time event-driven synchronization, has been advocated as an effective strategy for regulation of power grids with limits on transmission capacity [38].

One of the earliest approaches to the specific problem of synchronous rendezvous under low-range interaction constraints [19], leverages the structure of a bipartite interaction topology, and exploits the capability of robots to wait at designated rendezvous stations for their counterparts to arrive. Other approaches utilize coordination mechanisms in which robots that come into rendezvous can schedule the time and location of their next encounter [19], [35]. However, When the robot motion is dictated primarily by exogeneous dynamics and onboard power is a scarce resource, as it is the case here, robots may not have the ability to wait in place, ensure initial connectivity to be able to cooperatively plan their next move, or rely on their own actuation capacity [39] to achieve rendezvous. Without specific assumptions on the structure of the underlying intermittently connected communication network, collective synchronization is likely to be dependent on global connectivity conditions [9], [34].

Within the pre-established context of intermittent very-short-range interaction and synchronous periodic rendezvous, the approach outlined in this paper differs in some key aspects: (i) the robot gross motion behavior is dominated by the ambient environmental dynamics forces, and the robotic agent actuation and coordination law has limited impact on it; and (ii) the communication topology is also heavily dependent on environmental dynamics, and connectivity of the overall network is not guaranteed. The reported approach therefore addresses this new problem instance through a novel, distributed control law that combines leader-following multi-robot coordination (cf. [9], [30], [40]) for periodic rendezvous with connectivity maintenance (cf. [34], [41]). The stability and asymptotic properties of the closed-loop networked system are formally established via an analysis based on a discrete-time invariance principle approach [42] that explicitly incorporates the geophysical environmental dynamics.

The rest of the paper is organized as follows. Section II describes the technical parameters of the robot control problem and frames it mathematically. Section III outlines the solution approach and formally establishes the stability and convergence properties of the closed-loop system. Section IV presents numerical results that corroborate the theoretical predictions of Section III, and adds some limited experimental evidence that suggests that the control architecture can be realized in practice despite the mismatch between the simplistic geophysical flow model and the actual environmental conditions. Section V concludes the paper.

II. Problem Formulation

Consider a regular planar arrangement of aligned reference frames, where each frame is centered at Cartesian coordinates $(\frac{s}{\pi}\ell_i, \frac{s}{\pi}m_i)$ for $i = 1, \dots, N$, such that for some $s > 0$, the quantities ${}^{s\ell_i}/\pi, {}^{sm_i}/\pi$ are integers. In this arrangement, the frames are positioned on a grid where each origin is displaced relative to the origin of a nearest neighboring frame by a distance s along either the first (ℓ) or the second (m) Cartesian coordinate.

Assume a polar coordinate parameterization $(\rho_i, \theta_i) \in \mathbb{R}_+ \times \mathbb{S}$ on frame i, and for a fixed $C \in (-1, 1)$ define a planar submanifold (henceforth referred to as orbit) around each center (ℓ_i, m_i) through the equation (see Fig. 2)

$$\cos\left(\tfrac{\pi}{s}\rho_i \cos\theta_i + \ell_i\right) \cos\left(\tfrac{\pi}{s}\rho_i \sin\theta_i + m_i\right) = \pm C \ . \quad (1)$$

Now fix the right hand side of (1) for each of the $i = 1, \dots, N$ frame origins to either $|C|$ or $-|C|$ so that neighboring (in the north/south/east/west direction)

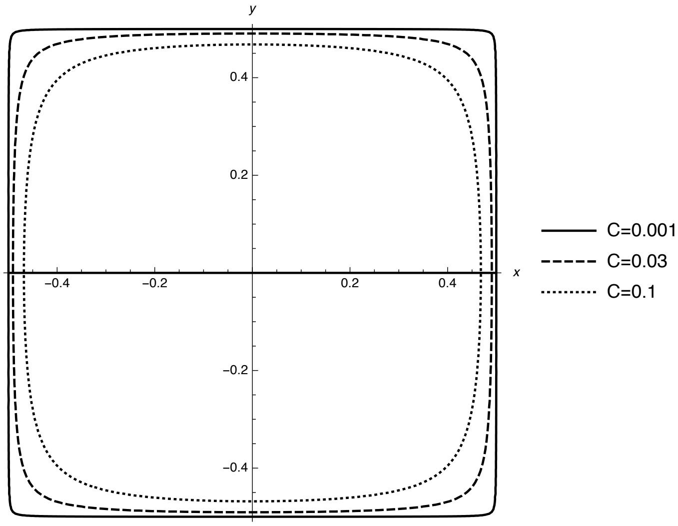

Fig. 2: Three different orbits, each for a different value of C around $(\ell, m) = (0, 0)$. As $C \to 0$ the orbit increasingly resembles a square.

frames are assigned opposite values. Then, setting a positive amplitude parameter $A > 0$, define the dynamics of an agent orbiting around (1) in the form

$$\begin{aligned} \dot{\theta}_i = f(\theta_i) \triangleq \\ -\operatorname{sgn}(C)\tfrac{\pi A}{\rho_i}\Big[\cos\theta_i\ \sin(\tfrac{\pi\rho_i}{s}\cos\theta_i)\cos(\tfrac{\pi\rho_i}{s}\sin\theta_i) \\ +\sin\theta_i\ \sin(\tfrac{\pi\rho_i}{s}\sin\theta_i)\cos(\tfrac{\pi\rho_i}{s}\cos\theta_i)\Big] \quad , \qquad (2) \end{aligned}$$

with a period of oscillation

$$T = \frac{8}{\pi A}\int_{\frac{s\arcsin\sqrt{C}}{\pi}}^{\pi/2} \frac{1}{\sqrt{\sin\frac{\pi x}{s} - C^2}}\,\mathrm{d}x \ .$$

Note that θ_i and ρ_i are coupled through (1). Depending on the sign of C, (2) forces the agent to drift either clockwise (for $C > 0$) or counter-clockwise (for $C < 0$). The dynamics above is motivated by the geophysical gyre flow model of [13], [20], [43].

Agents moving in neighboring orbits i and j, i.e. satisfying either $\ell_i - \ell_j = \pm s\pi$ or $m_i - m_j = \pm s\pi$, may come into *rendezvous* as they orbit around their (gyre) centers if their Cartesian coordinates relative to any fixed frame (either i or j) are within a distance $\delta \ll s$.

Given the shape of the gyre orbits (1) for $|C| \to 0$ and the fact that $\delta \ll s$, the proximity condition for rendezvous is satisfied for two neighboring agents drifting along orbits i and j in two distinct scenarios:

(i) the agents are moving on the sides of their corresponding rounded square-shaped orbits, in which case for some small $\varepsilon > 0$, $|\theta_i + \theta_j - (2k+1)\pi| < \varepsilon$ or $|\theta_i + \theta_j - 2k\pi| < \varepsilon$, or
(ii) the agents are near the rounded corners of their orbits (where θ_i would be close to $(2k+1)\frac{\pi}{4}$) in which case $|\theta_i - \theta_j - (2k+1)\pi| < \varepsilon$.

In case (i) exactly two agents are in rendezvous within each ball of radius δ, whereas in case (ii) up to four agents can be in rendezvous with each other.

Agents interact with each other *only* when they are in rendezvous. When they are not in rendezvous, they simply drift along their orbits following (2). When they are in rendezvous, however, their dynamics change to

$$\dot{\theta}_i = f_C(\theta_i) + u_i \ , \qquad (3)$$

where u_i may depend on the phases θ_j of the agents who are in rendezvous with i.

The dynamics of (assume non-interacting) agents (2) steer agents along their corresponding orbits (1) in directions dictated by the sign of the constant on the right hand side of (1). Neighboring agents i and j orbiting centers $(\frac{s}{\pi}\ell_i, \frac{s}{\pi}m_i)$, $(\frac{s}{\pi}\ell_j, \frac{s}{\pi}m_j)$ respectively, with $|\ell_i - \ell_j| = s\pi$ or $|m_i - m_j| = s\pi$, will rotate in opposite directions. To facilitate comparisons between phases of neighboring agents, we propose projecting their orbital positions on a common virtual orbit, in which all of them move in the same direction. The projection is implemented as follows.

Pick an arbitrary orbit in the grid, centered at (ℓ_i, m_i), as the common virtual orbit, and assume that for this gyre flow, $C > 0$. For any other orbit surrounding a center (ℓ_j, m_j) locate the agent moving on it, and project an image of the orbital position of this agent to a neighboring orbit that is closer to that around (ℓ_i, m_i) row- or column-wise (it does not matter whether you move along a row or a column), symmetrically to the axis of symmetry separating the two neighboring orbits. Notice now that the mirrored image is moving with the orientation of the resident agent to this orbit. Repeat this process until the remote image of agent j is now on the common orbit i, and denote ϑ_j the phase of that remotely projected image of agent j. From this point on, ϑ_j will be representing agent j on the common orbit i. To simplify notation going forward we will drop the subscript C from the right hand side of (3) when referring to the phase image motion on the common virtual orbit, and write

$$\begin{aligned} \dot{\vartheta}_j &= -\tfrac{\pi A}{\rho_j}\Big[\cos\vartheta_j\ \sin(\tfrac{\pi\rho_j}{s}\cos\vartheta_j)\cos(\tfrac{\pi\rho_j}{s}\sin\vartheta_j) \\ &\qquad +\sin\vartheta_j\ \sin(\tfrac{\pi\rho_j}{s}\sin\vartheta_j)\cos(\tfrac{\pi\rho_j}{s}\cos\theta_j)\Big] + u_j \\ &= f(\vartheta_j) + u_j \ . \qquad (4) \end{aligned}$$

The control objective is to have $\vartheta_i(t) - \vartheta_j(t) \to 0$, for any $i, j \in \{1, \ldots, N\}$, as $t \to \infty$.

Remark 1. *The phase motion dynamic* (3) *stems from the dynamic in Cartesian coordinates [27].*

$$\dot{x} = \pi A\cos\tfrac{\pi}{s}x\sin\tfrac{\pi}{s}y + u_x \triangleq f(x, y) + u_x \qquad (5a)$$

$$\dot{y} = -\pi A\cos\tfrac{\pi}{s}y\sin\tfrac{\pi}{s}x + u_y \triangleq g(x, y) + u_y \qquad (5b)$$

III. Technical approach

For $i \in \{1, \ldots, N\}$, find ϑ_i such that $\forall j \in \{1, \ldots, N\} \setminus \{i\}$, $(\vartheta_i - \vartheta_j)_{\mathrm{mod}\,2\pi} \geq 0$. If there is more than one $i \in \{1, \ldots, N\} \setminus \{i\}$ such that $(\vartheta_i - \vartheta_j)_{\mathrm{mod}\,2\pi} \geq 0$, pick one of those solutions arbitrarily and define $\vartheta_{\max} \triangleq$

ϑ_i. Then for $k \in \{1,\dots,N\}$, find ϑ_k such that $\forall j \in \{1,\dots,N\} \setminus \{k\}$, $(\vartheta_k - \vartheta_j)_{\mathrm{mod}\,2\pi} \leq 0$. Similarly, if more than one solutions ϑ_k satisfy the above inequality, pick arbitrarily one and set $\vartheta_{\min} \triangleq \vartheta_k$. In this sense, the relation $(\vartheta_i - \vartheta_j)_{\mathrm{mod}\,2\pi} \geq 0 \iff \vartheta_i \geq_{\mathrm{mod}\,2\pi} \vartheta_j$ defines a total order on $\{\vartheta_i,\dots,\vartheta_N\}$. Since agents travel on their orbits with a common frequency, after one period they will have met all agents that they will be coming in periodic rendezvous with.

Consider two agents i, j, moving on neighboring orbits and having phase images on the common virtual orbit denoted ϑ_i, ϑ_j, respectively. Each phase image evolves according to (4) for the special case where $u_i = u_j = 0$. The absolute value of their phase difference, $|\Delta\vartheta_{ij}| \triangleq |\vartheta_i - \vartheta_j|$ is a time-varying yet periodic quantity which oscillates between two extremal values $\min|\Delta\vartheta_{ij}|$, and $\max|\Delta\vartheta_{ij}|$ with period T. The geometry of the orbit (1) and the dynamics on it (2) suggest that the extremal values are attained at specific configurations: $\min|\Delta\vartheta_{ij}|$ is attained when $\vartheta_i + \vartheta_j = {}^{(2k+1)\pi}/_4$, and $\max|\Delta\vartheta_{ij}|$ when $\vartheta_i + \vartheta_j = {}^{k\pi}/_2$, for $k \in \mathbb{Z}$.

One way for one to see that is to consider the distribution of the agent's speed $v = \sqrt{\dot{x}^2 + \dot{y}^2}$ along the orbit (1) for $(\ell, m) = (0,0)$ and $y \to \frac{s}{2}$. In the limit, as $C \to 0$, the speed v takes the form

$$\lim_{C\to 0} v = \pi A \left|\cos\left(\frac{\pi x}{s}\right)\right| \quad , \tag{6}$$

and when the agent approaches the vertical sides of its orbit, that is when $x \to \pm 0.5s$ in the configuration depicted in Fig. 2, the speed drops to a minimum—of 0 in the limit case of $C = 0$ as indicated in (6), which means that the agent essentially stops. The function that maps the agent's single degree of freedom to its speed over the orbit is highly nonlinear for a general case of C. Due to continuity, however, we can reasonably expect the speed function to behave similarly as described above for cases of C in the neighborhood of zero, namely agents maintaining some (small) speed as they slowly traverse the orbit corner—see Fig. 3.

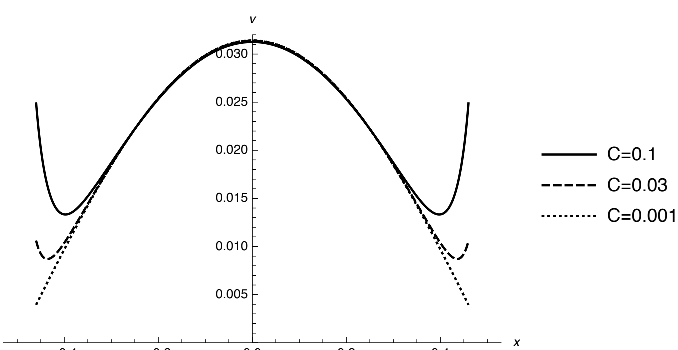

Fig. 3: The profile of the agent's speed v, as a function of the Cartesian coordinate x, along the top side of the orbit featured in Fig. 2. The agent's motion is symmetric on each of the four sides. Close to the orbit "corners," the agent slows down, and the reduction in speed there is larger the closer parameter C is to zero.

Now imagine two agents i and j moving on the same orbit in the neighborhood of an orbit corner, and with i having a small lead over j. A first case would be when i and j are converging to the corner. Then as i approaches the corner of the orbit it will slow down faster than j, and therefore their distance on the orbit will decrease monotonically—as a result their phase difference will decrease to, that is $|\Delta\vartheta_{ij}| \to 0$. The alternative case is when i and j are both moving away from a corner. Then i will accelerate more than j and thus their distance on the orbit will increase monotonically. Therefore, with the pair of agents on either side of the orbit corner, $|\Delta\vartheta_{ij}|$ will decrease as they approach the corner, and increase as they depart, suggesting that at the corner, i.e., the configuration where $\vartheta_i + \vartheta_j = {}^{(2k+1)\pi}/_4$, $|\Delta\vartheta_{ij}|$ attains its minimum.

In order for neighboring agents i and j to reach rendezvous, their phase difference needs to be small enough so that the agents' Euclidean distance falls below the threshold δ. Due to the nonlinear character of the orbit (1) and its vector field (2), necessary and sufficient conditions for rendezvous are not straightforward. Instead, sufficient conditions will be provided, in the form of the following proposition.

Proposition 1 (Sufficient condition for rendezvous on gyres)**.** *Let i and j be the indices of two agents moving on adjacent orbits, and ϑ_i, ϑ_j be their phase images, respectively, on the common virtual orbit. Denote $\Delta\vartheta_{ij}(t_0) = \vartheta_i(t_0) - \vartheta_j(t_0)$ the agents' phase image difference at some initial time instant t_0. The agents will rendezvous if*

$$\min_{t_0 \leq t \leq t_0+T} |\Delta_{ij}\vartheta(t)| < 2\left(\frac{\pi}{4} - \arctan(1 - \frac{\delta}{s})\right) \quad . \tag{7}$$

Proof. Since $|\Delta\vartheta_{ij}|$ attains its minimum where ${}^{(\vartheta_i+\vartheta_j)}/_2 = {}^{(2k+1)\pi}/_4$ for $k \in \mathbb{Z}$, it makes sense to focus on these configurations: if rendezvous does not happen there, it will not happen anywhere. Rendezvous happens when two agents find themselves within a δ (Euclidean) distance while in orbit. The problem is now constrained further as follows: Consider a ball (circle) of radius ${}^{\delta}/_2$ around the point of symmetry in between four adjacent gyre orbits (which is in fact a saddle point for the surrounding flow) (Fig. 4). Admittedly, two agents flowing along neighboring orbits can come within δ distance even without being both in this ball centered at the symmetry point. Still, this analysis is conservative in the sense that if i and j cannot decrease their distance below δ, they will not coexist in the ball of Fig. 4; however, if they coexist in this ball they will sure have achieved rendezvous.

For the sake of this conservative analysis, assume for the moment that rendezvous occurs when agents coexist in the ball of Fig. 4. The figure depicts a four-agent configuration at a location where ${}^{(\vartheta_i+\vartheta_j)}/_2 \approx {}^{(2k+1)\pi}/_4$, and in particular, a case where the three agents j, n, and p, are about to miss their rendezvous with agent i. The reason is that i exits the ball right as j, n, and p are just entering. Notice that in these extremal configurations, (a) the phase images of agents j, n, and p on the orbit

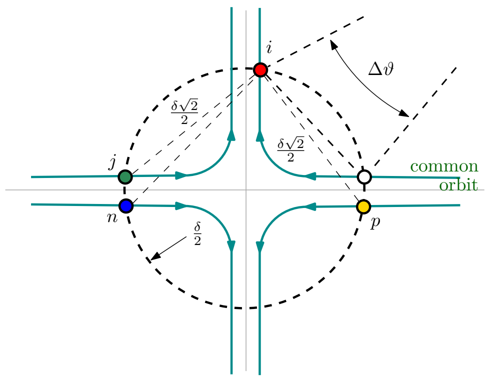

Fig. 4: Gyre detail around a flow saddle point with four agents in rendezvous.

of agent i (assumed to be the common virtual orbit), will coincide; and (b) the distances between i and all the other agents are at least as big as the distance between i and their common phase image, which is a bit less than $\delta\sqrt{2}/2$. It follows, therefore, that if i and j have phase images that are less than $\delta\sqrt{2}/2$ from each other, they will achieve rendezvous even for a short time interval. (Recall that $|\Delta\vartheta_{ij}|$ reaches a minimum when ϑ_i and ϑ_j position themselves symmetrically relative to $(2k+1)\pi/4$, so if the images are such that the spatial distance is less than $\delta\sqrt{2}/2$ anywhere else on the common orbit the distance will be even smaller near the corners of Fig. 4 for $\delta/s < 1/2$.) Given that $\delta \ll s$, rendezvous will not be possible unless the neighboring orbits are much closer than δ (which happens for $|C|$ close to zero), in which case the difference of the Euclidean distance between the images of i and j and $\delta\sqrt{2}/2$ will be negligible, and since the agents will in fact be already be in rendezvous (within distance δ) by the time their images' spatial distance drops to $\delta\sqrt{2}/2$, this approximation is deemed acceptable. The phase difference $\Delta\vartheta$ that corresponds to a chord of length $\delta\sqrt{2}/2$ on the circle of radius $\delta/2$ around the point of symmetry is $2[\frac{\pi}{4} - \arctan(1-\frac{\delta}{s})]$. □

Let the agents within a group that is in rendezvous establish *leader-follower relationships*. Specifically, an agent will "follow" any other agent it meets provided that this other agent has larger phase image than its own. For an agent $j \in \{1,\dots,N\}$, the agents that it follows form a set $\mathcal{L}_j$, while the agents following j are indexed in set $\mathcal{F}_j$.

However, agent j can follow only its leaders that it is currently in rendezvous with. Then, its actuation input (with reference to (4)) is activated and follows the control law

$$u_j = -\sum_{i\in\mathcal{L}_j(t)} a_{ij}\,(\vartheta_j - \vartheta_i)_{\mathrm{mod}\,2\pi}\ , \tag{8}$$

where a_{ij} is a positive control gain.

The number of different groups of agents that can come into rendezvous over the course of a period is finite, and can be indexed from a set $\mathcal{I} \subset \mathbf{2}^N$. Set $\mathcal{I}$ is made time-invariant by tasking each agent j who is a leader to preserve its followers $\mathcal{F}_j$. This is done by ensuring that a leader does not increase its phase difference to its followers beyond the point that it will prevent it from achieving rendezvous with them again. The reason this works is because whether two agents moving on neighboring orbits under their unforced dynamics (2) will rendezvous within one period T, depends on their relative difference between their phases (Proposition 1). The connectivity maintenance control is therefore implemented as follows:

Proposition 2 (Connectivity preservation)**.** *Let i be an agent who is both a leader in some group(s) and a follower in other(s). Denote t_j the time instant when follower $j \in \mathcal{F}_i$ breaks from its rendezvous with leader i. If over the course of one period T, the actuation-induced phase lead relative to its unactuated orbit flow dynamics* (2)*, is restricted according to*

$$\int_{t_0}^{t_0+T} u_i(t)\,\mathrm{d}t < 2\left(\frac{\pi}{4} - \arctan(1-\frac{\delta}{s})\right) - \max_{j\in\mathcal{F}_i} |\vartheta_i(t_j) - \vartheta_j(t_j)| \tag{9}$$

then the leader-follower relationships in which i is the leader, are preserved.

Proof. When agents in rendezvous are completely in synch, implying that they enter and exit the ball or radius $\delta/2$ around the flow saddle point (see Proposition 1), then their phase images on the common orbit coincide. If, on the other hand, (under the conservative conditions of Proposition 1) they are on the verge of missing their rendezvous window, then their phase images have a difference of at least $2[\frac{\pi}{4} - \arctan(1-\frac{\delta}{s})]$. Over the course of one period of oscillation, T, the phase image differences between i and its followers reach their minima when the images on the common orbit are closest to and symmetric to the diagonal linking the center of the common orbit to one of its rounded corners (Fig. 4). According to Proposition 1, this minimal difference should not exceed $2[\frac{\pi}{4} - \arctan(1-\frac{\delta}{s})]$, because then the agents are in risk of missing their rendezvous window. Assuming now that the followers of i, $\mathcal{F}_i$ do not themselves accelerate relative to their orbit dynamics after they break rendezvous with i—if they do, the bound of (9) will be more conservative than needed for connectivity maintenance—then i should restrict its own relative acceleration so that the phase lead it achieves with respect to its natural orbit flow, plus the minimum phase difference to its most lagging follower does not exceed $2[\frac{\pi}{4} - \arctan(1-\frac{\delta}{s})]$. One thus arrives at $\int_{t_0}^{t_0+T} u_i(t)\,\mathrm{d}t < 2[\frac{\pi}{4} - \arctan(1-\frac{\delta}{s})] - \max_{j\in\mathcal{F}_i}\min_{t_0\le t\le t_0+T}|\vartheta_i(t) - \vartheta_j(t)|$. Note now that for a follower $j \in \mathcal{F}_i$, (see the discussion in the proof of Proposition 1) $\min_{t_0\le t\le t_0+T}|\vartheta_i(t) - \vartheta_j(t)| \le |\vartheta_i(t_j) - \vartheta_j(t_j)|$, where t_j is the time instant at which the connection between leader i and follower j was severed and their rendezvous terminated. Substituting $|\vartheta_i(t_j) - \vartheta_j(t_j)|$ for $\min_{t_0\le t\le t_0+T}|\vartheta_i(t) - \vartheta_j(t)|$ yields (9). □

Thus, every agent at rendezvous applies (8) (except for the group leader for which $\mathcal{L}_j = \varnothing$). They do so throughout the whole duration of the rendezvous, unless they risk breaking up their leader-follower relationship with some followers in $\mathcal{F}_j$ in other groups (if any). In such cases, agents terminate their actuation input prematurely and default to $u_j = 0$.

At a given time instant t, only a subset of the groups in $\mathcal{I}$ that are in rendezvous, and we denote this set using a set-valued piecewise constant function $\mathcal{R} : \mathbb{R}_+ \rightrightarrows \mathcal{I}$. The leader-follower relationships within a group that is in rendezvous can be naturally encoded into a directed graph $\mathcal{G} = (\mathcal{V}, \mathcal{E})$, then $\mathcal{V}$ will contain the indices of the agents in rendezvous, and $\mathcal{E}$ will contain ordered pairs of the form (i, j) with $i, j \in \mathcal{V}$ and the understanding that i follows neighboring agent j while this group is in rendezvous.

We will refer to a group of agents in rendezvous using its associated directed graph. At a particular instant in time t there can be several agent groups in rendezvous, each indexed using a unique element of the set $\mathcal{R}(t)$. Any of these groups will have cardinality either 2, 3, or 4, (see Section II) depending on which segment of their orbit they experience proximity with their neighbor(s). For an arbitrary group $\mathcal{G}_L$ with $L \in \mathcal{R}(t)$, consider the phase image stack vector $\boldsymbol{\vartheta}_L$ and denote L_m the dimension of $\boldsymbol{\vartheta}_L$.

Proposition 3. *While an agent group is in rendezvous, the phases of all its followers converge exponentially and* monotonically *to the phase of the group's leader.*

Proof. Collect the phase images of the agents within a group in rendezvous in a stack vector $\boldsymbol{\vartheta} \in \mathbb{S}^k$ for $k \in \{2, 3, 4\}$, and order the elements of $\boldsymbol{\vartheta}$ from largest to smallest. Without loss of generality assume that $\boldsymbol{\vartheta}_L$ can be decomposed in the form $\boldsymbol{\vartheta}_L = (\boldsymbol{\vartheta}_{-L},\ \vartheta_{L_m})^\intercal$, where ϑ_{L_m} is the phase image of the agent that does not have an outgoing edge in $\mathcal{E}_L$—this is the leader of the group, having the largest phase image. From (4) and (8) it follows that the dynamics of the group's phase images evolve as the solution of a linear nominal system subject to a nonlinear perturbation

$$\dot{\boldsymbol{\vartheta}}_L = \begin{bmatrix} A_{-L} & A_{L_m} \\ \mathbf{0}_{1\times(L_m-1)} & 0 \end{bmatrix} \begin{pmatrix} \boldsymbol{\vartheta}_{-L} \\ \vartheta_{L_m} \end{pmatrix} + \begin{pmatrix} \boldsymbol{f}(\boldsymbol{\vartheta}_{-L}) \\ f(\vartheta_{L_m}) \end{pmatrix} \ , \quad (10)$$

in which $\mathbf{0}_{n\times m}$ denotes the $n \times m$ zero matrix, $\boldsymbol{f}(\boldsymbol{\vartheta}_{-L})$ is the stack vector of the followers' unforced orbital dynamics (2) in the group, A_{L_m} is a column vector with nonnegative entries having at position $1 \le k \le L_m - 1$ the a_{ij} control gain associated with the leader-follower relationship of the agent whose phase image is in position k in the $\boldsymbol{\vartheta}_{-L}$ vector with the leader of the group, and A_{-L} is the $(L_m - 1) \times (L_m - 1)$ matrix whose entries are formed by the a_{ij} control gains of the leader-follower relationships among the group's followers. Specifically, the element of A_{L_m} in row p, column q is the control gain associated with this pair if the agent whose phase image at entry p of $\boldsymbol{\vartheta}_{-L}$ follows the agent whose phase image is in location q in $\boldsymbol{\vartheta}_{-L}$, while the diagonal elements of A_{-L} are the negated sums of all non-diagonal elements on that particular row plus the one in the same row of A_{L_m}. (This implies that the whole matrix in the right hand side of (10) is row stochastic.) Due to the total order that the set made of the elements of $\boldsymbol{\vartheta}_L$ will enjoy, the elements of $\boldsymbol{\vartheta}_{-L}$ can always be arranged so that A_{-L} is upper triangular, in which case its eigenvalues will be its (negative) diagonal elements.

Let I_n denote the n-dimensional identity matrix, let $\mathbb{1}_n$ be the n-dimensional vector of ones, and define a new (vector) variable

$$\boldsymbol{x}_L = \begin{bmatrix} I_{L_m-1} & -\mathbb{1}_{L_m-1} \end{bmatrix} \boldsymbol{\vartheta}_L \in \mathbb{S}^{L_m-1} \ , \quad (11)$$

which will evolve, given (10) and after setting $\Delta\boldsymbol{f}(\boldsymbol{x}_L, \vartheta_{L_m}) \triangleq \boldsymbol{f}(\boldsymbol{\vartheta}_{-L}) - f(\vartheta_{L_m})\mathbb{1}_{L_m-1}$, according to

$$\dot{\boldsymbol{x}}_L = A_{-L}\, \boldsymbol{x}_L + \Delta\boldsymbol{f}(\boldsymbol{x}_L, \vartheta_{L_m}) \ . \quad (12)$$

To see this, rewrite (11) as $\boldsymbol{\vartheta}_{-L} = \boldsymbol{x}_L + \vartheta_{L_m}\mathbb{1}_{L_m-1}$ and take derivatives using (10) to get

$$\begin{aligned} \dot{\boldsymbol{\vartheta}}_{-L} &= \dot{\boldsymbol{x}}_L + \dot{\vartheta}_{L_m}\mathbb{1}_{L_m-1} \\ &= \dot{\boldsymbol{x}}_L + f(\vartheta_{L_m})\mathbb{1}_{L_m-1} \\ &= \begin{bmatrix} A_{-L} & A_{L_m} \end{bmatrix} \begin{pmatrix} \boldsymbol{\vartheta}_{-L} \\ \vartheta_{L_m} \end{pmatrix} + \boldsymbol{f}(\boldsymbol{\vartheta}_{-L}) \\ &= \begin{bmatrix} A_{-L} & A_{L_m} \end{bmatrix} \left(\begin{pmatrix} \boldsymbol{x}_L \\ 0 \end{pmatrix} + \vartheta_{L_m}\mathbb{1}_{L_m} \right) + \boldsymbol{f}(\boldsymbol{\vartheta}_{-L}) \\ &= A_{-L}\boldsymbol{x}_L + \boldsymbol{f}(\boldsymbol{\vartheta}_{-L}) + \vartheta_{L_m} \begin{bmatrix} A_{-L} & A_{L_m} \end{bmatrix} \mathbb{1}_{L_m} \ , \end{aligned}$$

from which (12) follows because $\begin{bmatrix} A_{-L} & A_{L_m} \end{bmatrix}$ is row stochastic.

The dynamical system (12) is a (stable) linear system with a nonlinear perturbation: the eigenvalues of A_{-L}, which can be thought of as upper triangular, are all negative—in fact, (8) with (10) confirm that a diagonal element is equal to $-\sum_{i\in\mathcal{N}_j} a_{ij}$ for some $j \in \{1, \dots, N\}$. The $\Delta\boldsymbol{f}(\boldsymbol{x}_L, \vartheta_{L_m})$ is actually vanishing because when $\boldsymbol{x}_L = 0 \implies \boldsymbol{\vartheta}_{-L} = \vartheta_{L_m}\mathbb{1}_{L_m-1} \implies \boldsymbol{f}(\boldsymbol{\vartheta}_{-L}) = f(\vartheta_{L_m})\mathbb{1}_{L_m-1}$. This is why (12) can be made exponentially stable for a sufficiently large choice of a_{ij}; to see this in detail, consider a quadratic Lyapunov function candidate

$$V_L(\boldsymbol{x}_L) = \boldsymbol{x}_L^\intercal P_L \boldsymbol{x}_L \ ,$$

where P_L is the unique solution of the Lyapunov equation $P_L A_{-L} + A_{-L}^\intercal P_L = -I_{L_m-1}$. It can be verified that with A_{-L} being triangular, P_L will be diagonal, and its largest and smallest eigenvalues will be equal to $\lambda_{\max}(P_L) = -1/2\lambda_{\min}(A_{-L})$ and $\lambda_{\min}(P_L) = -1/2\lambda_{\max}(A_{-L})$, respectively.

Then invoking [44, Lemma 9.1], one concludes that (12) is exponentially stable.[1] Note, now that the nominal

[1] The bound on $\|\frac{\partial \Delta\boldsymbol{f}}{\partial \boldsymbol{x}_L}\|$ is given in the appendix.

(unperturbed) linear system has real eigenvalues providing exponential convergence with no oscillation for its state. The fact that the bound on the rate of increase of $\Delta \boldsymbol{f}$ is dominated by the rate of decrease of the state of the nominal system, especially given the triangular structure of A_{-L}, essentially ensures that the solutions of (12) not only decrease exponentially, but they do so monotonically. □

Note, however, that the limited time in which $\mathcal{G}_L$ is in rendezvous may not allow its state $\boldsymbol{x}_L$ to converge to the origin. In addition, (12) rendezvous intermittently. In between the rendezvous times of group $\mathcal{G}_L$, its agents may flow passively along (2), or rendezvous in other groups—in which case some of these interactions can potentially disrupt the convergence of $\mathcal{G}_L$. Between the times that $\mathcal{G}_L$ rendezvous, therefore, V_L does not necessarily decrease. This complication motivates an analysis of the whole network in discrete time, where a time step expresses the time interval between two subsequent rendezvous events occurring for agent groups which include the agent with the smallest phase image, namely $\vartheta_{\min}$.

In the forthcoming analysis of the stability properties of the network, the following lemma will be of use.

Lemma 1. *Consider two dynamical systems*

$$\dot{\bar{z}} = f(\bar{z}),\ \bar{z}(0) = \bar{z}_0; \qquad \dot{\underline{z}} = f(\underline{z}),\ \underline{z}(0) = \underline{z}_0 \tag{13a}$$

$$\dot{\bar{w}} = f(\overline{w}),\ \overline{w}(0) = \overline{w}_0; \quad \dot{\underline{w}} = f(\underline{w}),\ \underline{w}(0) = \underline{w}_0 \tag{13b}$$

where $\underline{z}_0 < \bar{z}_0$ and $\underline{w}_0 < \overline{w}_0$. Take $C < 0$ and assume that $\bar{z}_0 = \overline{w}_0$ and $\underline{z}_0 > \underline{w}_0$. Then,

$$\min_{t\in[0,T]} \left\{\bar{z}(t) - \underline{z}(t)\right\} < \min_{t\in[0,T]} \left\{\overline{w}(t) - \underline{w}(t)\right\} \ .$$

Proof. Since $\underline{z}$ and $\underline{w}$ evolve on the same periodic orbit with period T and $C < 0$, from uniqueness of solutions and given that $\underline{z}_0 > \underline{w}_0$ there will be an $\varepsilon > 0$, possibly time-varying, such that $\underline{w}(t+\varepsilon) = \underline{z}(t)$, while $\underline{z}(t) > \underline{w}(t)$, $\forall t \geq 0$. At the same time, $\bar{z}(t) = \overline{w}(t)$, $\forall t \geq 0$. In light of these observations,

$$\begin{aligned} &\overline{w}(t) + \underline{w}(t) < \bar{z}(t) + \underline{z}(t) \quad \forall t \geq 0 \implies \\ &\quad t_w \triangleq \inf\left\{ t \geq 0 \mid \tfrac{\overline{w}+\underline{w}}{2} = \tfrac{(2k+1)\pi}{4}, k \in \mathbb{N}\right\} > \\ &\qquad t_z \triangleq \inf\left\{ t \geq 0 \mid \tfrac{\bar{z}+\underline{z}}{2} = \tfrac{(2k+1)\pi}{4}, k \in \mathbb{N}\right\} \ , \end{aligned}$$

meaning that (13a) will reach $\min\{\bar{z} - \underline{z}\}$ faster than (13b) will reach $\min\{\overline{w} - \underline{w}\}$. Given that $\overline{w}(t) = \bar{z}(t)$, this implies that $\bar{z}(t_z) < \overline{w}(t_w)$. As a result,

$$\begin{aligned} \min_{t\in[0,T]} \left\{\bar{z}(t) - \underline{z}(t)\right\} &= 2\left(\bar{z}(t_z) - \tfrac{(2k+1)\pi}{4}\right) \\ &< 2\left(\overline{w}(t_w) - \tfrac{(2k+1)\pi}{4}\right) = \min_{t\in[0,T]} \left\{\overline{w}(t) - \underline{w}(t)\right\} \end{aligned}$$

Summing up,

$$\begin{aligned} &\bar{z}_0 = \overline{w}_0,\ \underline{z}_0 > \underline{w}_0 \implies \\ &\quad \min_{t\in[0,T]} \left\{\bar{z}(t) - \underline{z}(t)\right\} < \min_{t\in[0,T]} \left\{\overline{w}(t) - \underline{w}(t)\right\} \ . \end{aligned} \tag{14}$$

□

The main result is summarized in the theorem that follows. The theorem states that as long as the leader-follower relationships form a spanning tree across the network, asymptotically all agents will achieve periodic rendezvous at different neighborhoods but *simultaneously*.

Theorem 1 (Network syncrhonization)**.** *If a collection of N agents with dynamics* (3) *evolving in a pattern of periodic orbits* (1) *under intermittent control law* (8)*, rendezvous periodically according to* (7) *and form leader-follower relationships encoded in a directed graph which has a time-invariant spanning tree after ensuring* (9)*, then the agents will eventually synchronize their phase image dynamics* (4) *and have them converge to that of the agent with the largest phase image.*

Proof. While the identity of the agent associated with $\vartheta_{\min}$ may change over time as different groups synchronize in a decentralized way, by nature of the interaction law (8), the identity of the agent associated with $\vartheta_{\max}$ is constant. The phase image of the agent associated with $\vartheta_{\max}$ evolves according to (4) with $u_j = 0\ \forall t \geq 0$.

Denote t_n beginning of the n^{th} time interval when the group containing the agent exhibiting $\vartheta_{\min}$ is in rendezvous. Let $\hat{\vartheta}(t)\mid_n$ denote the solution of (2) with initial condition $\hat{\vartheta}(0)\mid_n = \vartheta(t_n)$, and define

$$V(n) \triangleq \min_{t\in[0,T]} \left\{\hat{\vartheta}_{\max}(t)\mid_n - \hat{\vartheta}_{\min}(t)\mid_n\right\} \ . \tag{15}$$

Recall that this minimum is attained when $(\hat{\vartheta}_{\max} + \hat{\vartheta}_{\min})/2 = (2k+1)\pi/4$. The value of this minimum is not known in closed form; what can be shown, however, Lemma 1 guarantees that the smaller the difference $\vartheta_{\max}(t_n) - \vartheta_{\min}(t_n)$ is, the smaller $V(n)$ would be. At the same time, Proposition 3 ensures that during rendezvous, $\vartheta_{\min}$ converges monotonically to some (higher) ϑ_{L_m} which also evolves according to (4) with $u_j = 0$ *during this rendezvous*. That implies that $\vartheta_{\min}$ *accelerates* relative to the unactuated flow dynamics (2) that always drive $\vartheta_{\max}$, and therefore reduces the difference $\vartheta_{\max} - \vartheta_{\min}$. As a result, if that rendezvous instance is indexed n, at the end of their rendezvous, say time t', the group that had the agent associated with $\vartheta_{\min}$ will have this agent presenting a phase image $\vartheta'_{\min}$ for which $\vartheta_{\max}(t') - \vartheta'_{\min}(t') < \vartheta_{\max}(t_n) - \vartheta_{\min}(t_n)$. In the above, the phase image of the trailing agent is primed to express the fact that by the end of the rendezvous interaction in that group, the agent with the minimum phase image may have changed.

However, irrespectively of whether the identity of the agent associated with $\vartheta_{\min}$ changes during a rendezvous period, as long as $t_{n+1} - t_n > 0$,[2] it will still be the case

[2]In fact, the possibility of $t_{n+1} = t_n$, $\forall n \in \mathbb{N}$ (an event time set with infinite cardinality) is excluded based on two facts: (i) by continuity, rendezvous times are always nonzero, and (ii) by definition, if there are multiple solutions to $\arg\min \vartheta_i$ then one is arbitrarily selected to define the agent with $\vartheta_{\min}$.

that when the next rendezvous involving $\vartheta_{\min}$ occurs, one has $\vartheta_{\max}(t_{n+1}) - \vartheta_{\min}(t_{n+1}) < \vartheta_{\max}(t_n) - \vartheta_{\min}(t_n)$. As a result,

$$\hat{\vartheta}_{\max}(0)\,|_{n+1} - \hat{\vartheta}_{\min}(0)\,|_{n+1} < \hat{\vartheta}_{\max}(0)\,|_{n} - \hat{\vartheta}_{\min}(0)\,|_{n} \ .$$

The differences $\hat{\vartheta}_{\max}(0)\,|_{n+1} - \hat{\vartheta}_{\min}(0)\,|_{n+1}$ and $\hat{\vartheta}_{\max}(0)\,|_{n} - \hat{\vartheta}_{\min}(0)\,|_{n}$ can be thought of as being the differences between the initial conditions of the two states in systems (13a) and (13b), respectively. Consequently, Lemma 1 will imply that

$$\min_{t\in[0,T]} \left\{\hat{\vartheta}_{\max}(t)\,|_{n+1} - \hat{\vartheta}_{\min}(t)\,|_{n+1}\right\} < \min_{t\in[0,T]} \left\{\hat{\vartheta}_{\max}(t)\,|_{n} - \hat{\vartheta}_{\min}(t)\,|_{n}\right\} \ , \quad (16)$$

suggesting that $V(n+1) < V(n)$.

Function $V(n)$, as defined in (15), is bounded, non-negative and continuous. Furthermore, since the agent associated with $\vartheta_{\max}$ will remain unactuated, while the one giving $\vartheta_{\min}$ will certainly accelerate on its first rendezvous, $\vartheta_{\max}(t_n) - \vartheta_{\min}(t_n) \le \vartheta_{\max}(t_1) - \vartheta_{\min}(t_1)$, meaning that the set in which $\vartheta_{\max}(t_n) - \vartheta_{\min}(t_n)$ and therefore $\hat{\vartheta}_{\max}(t)\,|_{n} - \hat{\vartheta}_{\min}(t)\,|_{n}$ takes values, is compact. Therefore, there exists a $c \ge 0$ such that as $n \to \infty$,

$$\left(\vartheta_{\max}(t_n) - \vartheta_{\min}(t_n)\right) \to M \cap V^{-1}(c) \ ,$$

where

$$V^{-1}(c) \triangleq \{\vartheta_{\max}(t_n) - \vartheta_{\min}(t_n) \in \mathbb{S}^1 \mid \min_{t\in[0,T]} \{\hat{\vartheta}_{\max}(t)\,|_{n} - \hat{\vartheta}_{\min}(t)\,|_{n}\} = c\}$$

and M is the largest invariant set in

$$E \triangleq \Big\{\vartheta_{\max}(t_n) - \vartheta_{\min}(t_n) \in \left[0, \vartheta_{\max}(t_1) - \vartheta_{\min}(t_1)\right] : \min_{t\in[0,T]} \left\{\hat{\vartheta}_{\max}(t)\,|_{n+1} - \hat{\vartheta}_{\min}(t)\,|_{n+1}\right\} - \min_{t\in[0,T]} \left\{\hat{\vartheta}_{\max}(t)\,|_{n} - \hat{\vartheta}_{\min}(t)\,|_{n}\right\} = 0\Big\} \ .$$

One can recall the monotonicity properties of

$$min_{t\in[0,T]} \left\{\hat{\vartheta}_{\max}(t)\,|_{n} - \hat{\vartheta}_{\min}(t)\,|_{n}\right\}$$

with respect to $\vartheta_{\max}(t_n) - \vartheta_{\min}(t_n)$ (see (14)) to conclude that E is equivalently expressed as

$$E = \Big\{\vartheta_{\max}(t_n) - \vartheta_{\min}(t_n) \in \left[0, \vartheta_{\max}(t_1) - \vartheta_{\min}(t_1)\right] : \vartheta_{\max}(t_{n+1}) - \vartheta_{\min}(t_{n+1}) = \vartheta_{\max}(t_n) - \vartheta_{\min}(t_n)\Big\} \ .$$

Now given the rendezvous group $\mathcal{G}_L$ dynamics (10) (for any arbitrary $L \in \mathcal{R}(t)$) and its stability properties established in Proposition 3, the difference $\vartheta_{\max}(t_n) - \vartheta_{\min}(t_n)$ will be time-invariant only if $\boldsymbol{\vartheta}_{-L} = 0$, which implies that $\vartheta_{\min} = \vartheta_{L_m}$. The phase image ϑ_{L_m}, however, has dynamics of its own: as long as the agent network has a spanning tree, the agent with ϑ_{L_m} is a follower in some other rendezvous group, ϑ_{L_m} converges to some other leading phase image, and from the network's percistent connectivity one inductively arrives at $\vartheta_{\min} = \vartheta_{\max}$. If $\vartheta_{\min} = \vartheta_{\max}$ and $\vartheta_{\min} \le \cdots \le \vartheta_i \le \vartheta_{\max}$ this inevitably means that $\vartheta_i = \vartheta_j$, $\forall i, j \in \{1, \ldots, N\}$, which is the only time-invariant configuration as t and n tend to infinity. □

IV. Validation

A. Numerical Simulation Analysis

We start with a small-scale numerical study of 3×3 grid arrangement of nine gyres (see e.g. the gyre arrangement in Fig. 5), each of which hosts one simulated drifter.

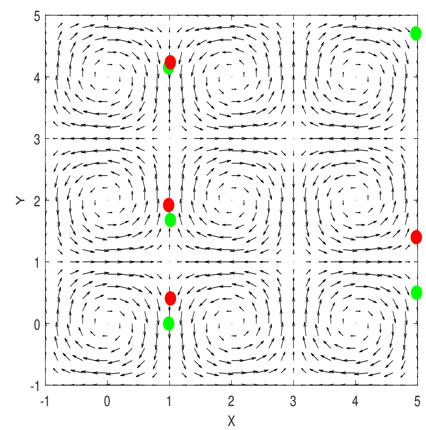

Fig. 5: An example of an arrangement of gyre flows on a grid. In this picture, each gyre occupies a 2×2 area and the flow lines within it resemble cocentric rounded squares. Drifters marked with different colors move in opposite orientations, following the direction of the vector fields inside their gyres.

The flow parameters chosen to realize the simulated geophysical flow for the small-scale study were $s = 2$, $\delta = 0.2$, and $A = 0.03$. The initial conditions used to produce the outcomes for the nine agents in Figs 6 and 7 are as follows. 1: (0.9873,0.0000); 2: (0.9872,1.9223); 3: (0.9869,4.1563); 4: (1.0137,4.2368); 5: (1.0145,1.6798); 6: (1.0159,0.4076); 7: (4.9820,0.5003); 8: (4.9784,1.4005); 9: (4.9714,4.7058).

The simulated start their motion from their assigned initial conditions moving along their orbit as it is prescribed by the flow equations (2), five of them rotating clockwise while the others counterclockwise. Until they come into distance δ from another robotic drifter and establish a first rendezvous with it, the robots do not apply any actuation; they just go with the flow. After being released and once they come into rendezvous they apply (8), fix their leader-follower relationships within their corresponding groups and start to reduce the differences between their phase images.

For this configuration, the evolution of the Lyapunov-like function $V(n)$ over time is depicted in Fig. 6. Figure 7, on the other hand, illustrates the frequency, duration, and scope of rendezvous events at the four (internal) flow saddle points, indicating how the rendezvous periodicity and duration time stabilizes to constant values over time.

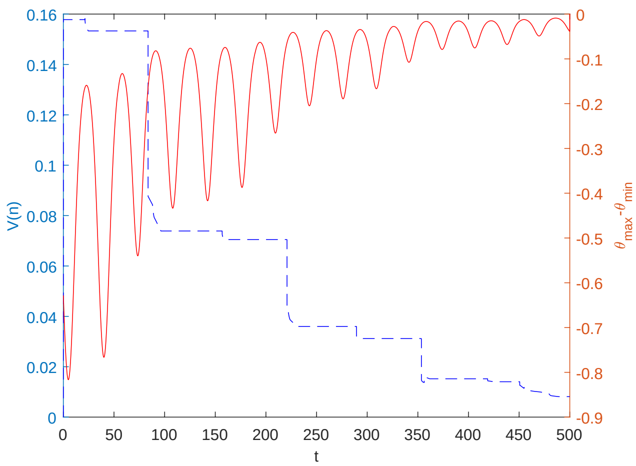

Fig. 6: Evolution of Lyapunov-like function $V(n)$ over the course of a simulation run (dashed curve), overlaid on the trajectory of $\vartheta_{\max}(t) - \vartheta_{\min}(t)$ (continuous curve). Function $V(n)$ decreases monotonically and its jumps coincide with the instances when the identity of the agent with $\vartheta_{\min}$ switches. The interval including four (same amplitude) peaks on the $\vartheta_{\max}(t) - \vartheta_{\min}(t)$ graph corresponds to one orbit period T, since along a virtual common orbit, the phase image difference is maximal along the four long sides based on (13).

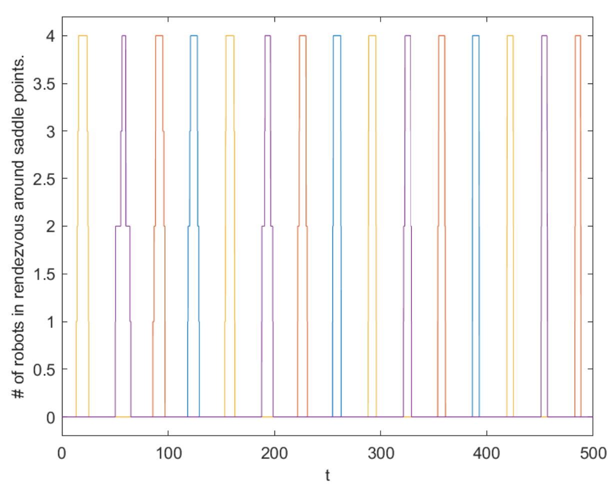

Fig. 7: The duration of rendezvous intervals around the flow saddle configurations over the course of network synchronization. The height of each pulse indicates the number of robots engaged in rendezvous and the width of the pulse expresses the duration of the rendezvous event at the saddle point. At steady state, this sequence of sets of saddle points in rendezvous repeats periodically at the period of the robots' orbit.

To verify the scalability properties of the synchronized rendezvous protocol, we created in silico a larger-scale planar pattern with 100 gyres arranged on a rectangular 10×10 grid. Gyre flow parameters A and s were now chosen at 0.03 and 1, respectively. In an attempt to accelerate the simulation, the rendezvous range δ was purposefully selected a relatively high at 0.4; the main reason for this is the appearance of accumulated numerical errors at lower C and δ regimes that pushed simulated robots away from their nominal orbits. On each gyre orbit associated to $C = 0.05$ (cf. Fig 2), we initialized a robotic drifter. With this choice of parameters, the period of oscillation T for a robotic drifter around each gyre orbit is about one minute ($T = 59.2275$ seconds, to be exact). We split the $[0, {}^{2\pi}/_3]$ interval into 100 values, and assigned initial conditions to the robots starting from the gyre centered at $(0, 0)$ and moving up and down, thus covering the grid from left to right in a raster scan fashion. This assignment method, compared to a completely random assignment, contributed giving initial intermittent connectivity to the network which is a necessary condition for synchronization—the network can preserve its connectivity but cannot establish it starting off without it. Naturally, this way it is $\vartheta_{\max}(0) - \vartheta_{\min}(0) = {}^{2\pi}/_3$.

Figure 8 shows the evolution of discrete-time Lyapunov-like function $V(n)$, from the start of the simulation with the initial conditions and for a period of 300 simulation seconds. Monotonic[3] convergence to zero for $V(n)$ is observed as simulation time $t \to \infty$.

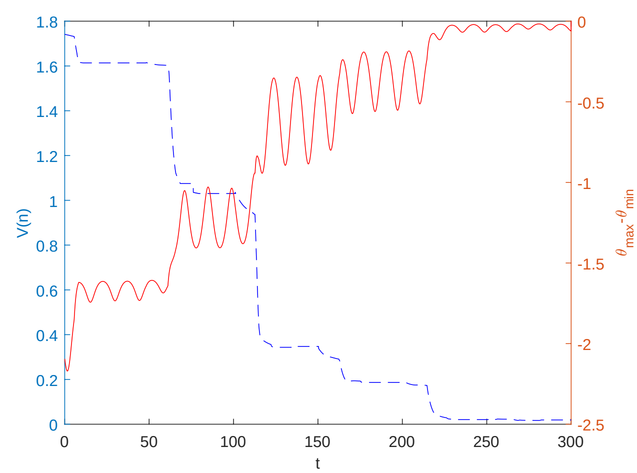

Fig. 8: Evolution of Lyapunov-like function $V(n)$ over the course of a simulation run (dashed curve), overlaid on the trajectory of $\vartheta_{\max}(t) - \vartheta_{\min}(t)$ (continuous curve). Function $V(n)$ decreases monotonically and its jumps coincide with the instances when the identity of the agent with $\vartheta_{\min}$ switches. The interval including four (same amplitude) peaks on the $\vartheta_{\max}(t) - \vartheta_{\min}(t)$ graph corresponds to one orbit period T, since along a virtual common orbit, the phase image difference is maximal along the four long sides based on (13).

If one observes the internal flow saddle points (where four rounded corners of neighboring gyres meet) and documents the scope and duration of the rendezvous

[3]There is, in fact, a very gradual decrease even along the apparent plateaus on the graph of $V(n)$, as the robot pair associated with $\vartheta_{\max} - \vartheta_{\min}$ remains fixed and $\vartheta_{\min}$ slowly crawls toward $\vartheta_{\max}$.

events occurring there, they will notice the following pattern. Initially, rendezvous events around these locations occur randomly and may include anywhere from 2 to 4 robots (Fig. 9). At steady state, all rendezvous events are periodic and last for equal time periods. Within the orbit period of about 60 seconds, as a robot goes around a full rotation on its orbit, it will rendezvous at all four saddle points with three other robots, in a sequence illustrated in the inset pictures on top of the rendezvous time evolution graph of Fig. 9.

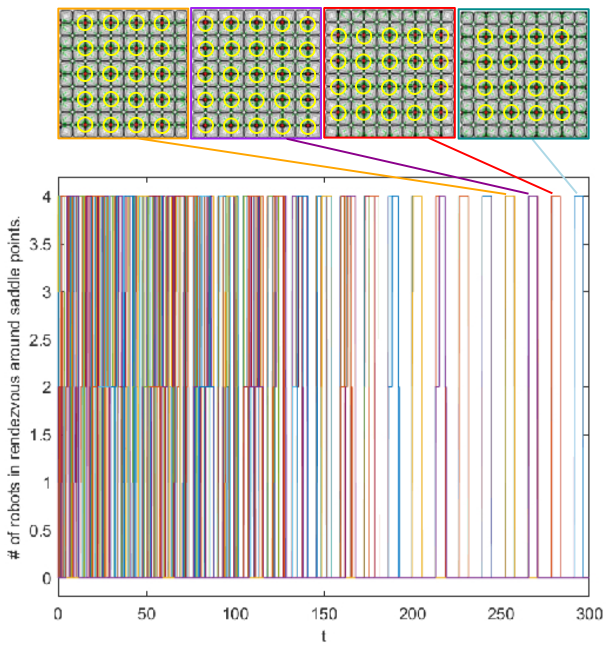

Fig. 9: The duration of rendezvous intervals around the flow saddle configurations over the course of network synchronization. The height of each pulse indicates the number of robots engaged in rendezvous and the width of the pulse expresses the duration of the rendezvous event at the saddle point. The insets on top of the graph mark (circled in yellow) the saddle point locations where robots are in rendezvous. At steady state, this sequence of sets of saddle points in rendezvous repeats periodically at the period of the robots' orbit.

B. Elements of Experimental Implementation

The numerical analysis of the previous section was based on the assumption that the robotic drifters follow their gyre orbits faithfully. In reality, no matter how strong the geophysical currents may be, there is considerable amount of noise and perturbation to throw them off course. Yet, keeping their motion on their designated orbit is important for achieving sustained synchronous rendezvous, because it affects the period of oscillation as well as their ability to come close enough to their neighbors to initiate interaction.

A pair of neighboring gyre flows was realized in laboratory conditions within a water tank steered by two submerged motor-driven propellers rotating in opposite directions (Fig. 10a). In this implementation, a robotic agent is realized in the form of the micro autonomous surface vehicle (mASV) of Fig. 10b which are localized externally through a motion capture system. As the plot of Fig. 11 indicates, the motion of the mASV within the current generated by the submerged propellers is noisy, and needs to be regulated in order to follow the nominal flow lines generated by the theoretical gyre model (1).

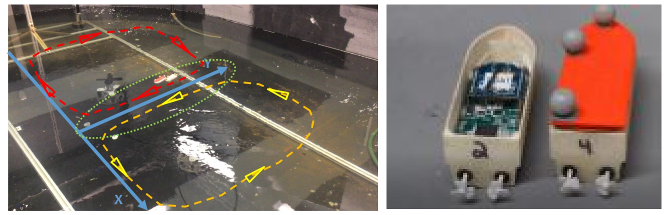

(a) (b)

Fig. 10: The experimental setup. (a) A view of the experimental multi-robot Coherent Structure Testbed (mCoSTe) at the University of Pennsylvania, where a pair of neighboring gyre flows with opposite orientation was realized; (b) A mASV which is differentially driven and can achieve a forward speed of up to 0.2 m/s (Courtesy of Prof. Ani Hsieh [27]).

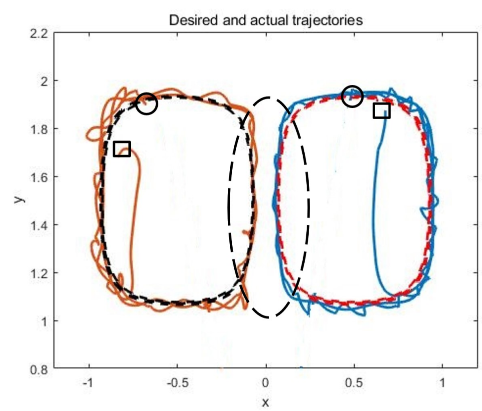

Fig. 11: Closed-loop motion of mASV (Fig. 10b) while attempting to track the designated surface paths (marked in Fig. 10a). Dashed curves represent the nominal flow lines that vehicles have to trace and solid lines show the mASVs' traversed paths. The square marker indicates the vehicles' initial position and the circle marks their final position. The dashed ellipsis highlights the region where the two vehicles rendezvous.

The remaining of this section, therefore, elaborates on a path tracking controller that can be implemented on differentially-driven micro-vehicles to follow the nominal flow lines of (1) with bounded errors in the presence of disturbances. Keeping the vehicle on the closed orbit associated with a specific value of parameter C is realized through a controller that acts on the radial component ρ of the vehicle's polar coordinates (ρ, θ) relative to the gyre's center.

The design of the radial regulation law u_ρ is based on the streamline-based control [4]. In this framework, *stream functions* quantify the path-independent net flow flux from one point P to another point Q. A quantification of this flux from P to Q is referred to as *stream* *value* and in the case of the geophysical flow considered here (see (5)) is expressed as $\psi_f(P,Q) \triangleq \int_P^Q f(x,y)\,\mathrm{d}y - g(x,y)\,\mathrm{d}x$. The set of points with the same stream value form a *streamline*. The actuated robotic drifter dynamics (5) can be seen as the result of a superposition of stream function $\psi_f(P,Q)$ with $\psi_d(P,Q) \triangleq \int_P^Q u_x\,\mathrm{d}y - u_y\,\mathrm{d}x$. In theory, a vehicle moving along a vector field (u_x, u_y) *relative* to a 2D incompressible flow field $(f(x,y), g(x,y))$ can only reach from P locations Q for which satisfy the (superimposed) *streamline constraint* $\psi_f(P,Q) + \psi_d(P,Q) = 0$ [4], and since by construction $\psi_f(P,Q) = 0$,[4] it follows that it should be $\psi_d(P,Q) = 0$. For the latter, it suffices that $u_x\,\mathrm{d}y - u_y\,\mathrm{d}x = 0$, which due (5), and after setting $R(x,y) \triangleq \tan\frac{\pi x}{s}(\tan\frac{\pi y}{s})^{-1}$, leads to the condition $u_y = -u_x P(x,y)$. From this condition, and given that

$$\begin{aligned} u_x &= u_\rho \cos\theta - u\,\rho\sin\theta \\ u_y &= u_\rho \sin\theta + u\,\rho\cos\theta \ , \end{aligned}$$

the radial regulation controller can be extracted as a function of the synchronization control law u_θ:

$$u_\rho = \rho\, u\, \frac{R(x,y)\sin\theta - \cos\theta}{R(x,y)\cos\theta + \sin\theta} \ .$$

V. Conclusion

One big challenge for large-scale ocean monitoring by marine vehicles with limited communication ability is how local interaction can result in a global synchronization so as to maximize the interaction time and realize global information transmission for all the agents in the network. At the same time, those low cost marine drifters should take advantage of the ambient flow field to perform the long endurance monitoring task. In this paper, the dynamic for a semi-passive drifter in dynamically dominant ambient ocean circulation is understood as a nonlinear periodic oscillation which is expressed in phase model. Constrained by the fact that a drifter can only perform local interaction with a relative small part of the network, we studied how to apply connectivity maintaining strategy to the network through design of controller. Local interaction accomplished through state feedback controller can successfully achieve local synchronization, which is proved by theory from stability of perturbed systems. Thanks to the connectivity maintaining theory and the achievement of local synchronization, the global synchronization can be possible. Based on the experimental result from small scale test tank, a orbit maintaining method is also designed. The numerical simulation supports the effectiveness of the synchronization strategy for a large network. Future work involves validation in experimental environment and how initial condition of the network influence the global synchronization result.

[4] To see this, set $u_x = u_y = 0$ for an unactuated vehicle, and apply the streamline constraint.

Appendix

Recall (11) $\boldsymbol{x}_L = \begin{bmatrix} I_{L_m-1} & -\mathbb{1}_{L_m-1}\end{bmatrix} \boldsymbol{\vartheta}_L \in \mathbb{S}^{L_m-1}$; then

$$\Delta\boldsymbol{f}(\boldsymbol{x}_L, \vartheta_{L_m}) \equiv \Delta\boldsymbol{f}\left(\left[\, I_{L_m-1} \ -\mathbb{1}_{L_m-1}\,\right]\boldsymbol{\vartheta}_L, \vartheta_{L_m}\right) = \Delta\boldsymbol{f}(\boldsymbol{\vartheta}_L) \ .$$

Therefore,

$$\frac{\partial\Delta\boldsymbol{f}}{\partial\boldsymbol{x}_L} = \frac{\partial\Delta\boldsymbol{f}}{\partial\boldsymbol{\vartheta}_L}\frac{\partial\boldsymbol{\vartheta}_L}{\partial\boldsymbol{x}_L} = \frac{\partial\Delta\boldsymbol{f}}{\partial\boldsymbol{\vartheta}_L}\begin{pmatrix} I_{L_m-1} \\ -\mathbb{1}^{\intercal}_{L_m-1}\end{pmatrix} \ .$$

At the same time,

$$\frac{\partial\Delta\boldsymbol{f}}{\partial\boldsymbol{\vartheta}_L} = \begin{bmatrix} \frac{\partial f(\vartheta_{L_1})}{\partial\vartheta_{L_1}} & 0 & \cdots & 0 \\ 0 & \frac{\partial f(\vartheta_{L_2})}{\partial\vartheta_{L_2}} & \cdots & 0 \\ & & \ddots & \\ 0 & \cdots & 0 & \frac{\partial f(\vartheta_{Lm})}{\partial\vartheta_{Lm}} \end{bmatrix} \ .$$

Given that the agents' phase images evolve on the (common) orbit $\cos\frac{\pi x}{s}\cos\frac{\pi y}{s} = C$, with $x = \rho\cos\vartheta$ and $y = \rho\sin\vartheta$, and with $\rho \in \left(\frac{s}{\pi}\arccos C, \frac{\sqrt{2}}{\pi}\arccos\sqrt{C}\right)$, the magnitude of each one of the diagonal elements

$$\left|\frac{\partial\Delta f(\vartheta_{L_i})}{\partial\vartheta_{L_i}}\right| = \Big|\frac{\pi^2 A}{s}\sin\frac{\pi x_{L_i}}{s}\cos\frac{\pi y_{L_i}}{s}\cos 2\vartheta_{L_i} - \frac{\pi A}{\rho_{L_i}}\left(\cos\frac{\pi x_{L_i}}{s}\sin\frac{\pi y_{L_i}}{s}\cos\vartheta_{L_i} - \sin\frac{\pi x_{L_i}}{s}\cos\frac{\pi y_{L_i}}{s}\sin\vartheta_{L_i}\right)\Big|$$

can be bounded as follows

$$\begin{aligned} \left|\frac{\partial\Delta f(\vartheta_{L_i})}{\partial\vartheta_{L_i}}\right| &\le \frac{\pi^2 A}{s}\left|\sin\frac{\pi x_{L_i}}{s}\sin\frac{\pi y_{L_i}}{s}\right| \\ &\quad + \frac{\pi A}{\rho_{L_i}}\sqrt{\cos^2\frac{\pi x_{L_i}}{s}\sin^2\frac{\pi y_{L_i}}{s} + \sin^2\frac{\pi x_{L_i}}{s}\cos^2\frac{\pi y_{L_i}}{s}} \\ &\le \frac{\pi^2 A}{s}\sqrt{1 + C^2 - \cos^2\frac{\pi x}{s} - \frac{C^2}{\cos^2\frac{\pi x}{s}}} \\ &\quad + \frac{\pi^2 A}{s\arccos C}\sqrt{\cos^2\frac{\pi x}{s} + \frac{C^2}{\cos^2\frac{\pi x}{s}} - 2C^2} \ . \end{aligned}$$

With $x \in \left[-\frac{s}{\pi}\arccos C, \frac{s}{\pi}\arccos C\right]$, the left hand side is maximized at $x = \pm\frac{s}{\pi}\arccos\sqrt{C}$, which yields the upper bound:

$$\left|\frac{\partial\Delta f(\vartheta_{L_i})}{\partial\vartheta_{L_i}}\right| \le \frac{\pi A}{s}\left(\pi(1-C) + \frac{\pi}{\arccos C}\sqrt{2C(1-C)}\right) \ .$$

It thus follows that

$$\left\|\frac{\partial\Delta\boldsymbol{f}}{\partial\boldsymbol{x}_L}\right\| \le \frac{\pi A\sqrt{10+2\sqrt{21}}}{2s}\left(\pi(1-C) + \frac{\pi}{\arccos C}\sqrt{2C(1-C)}\right).$$

References

[1] J. Hansen, S. Manjanna, A. Q. Li, I. Rekleitis, and G. Dudek, "Autonomous Marine Sampling Enhanced by Strategically Deployed Drifters in Marine Flow Fields," in *Proceedings of MTS/IEEE OCEANS*, pp. 1–7, 2018.

[2] M. A. Hsieh, H. Hajieghrary, D. Kularatne, C. R. Heckman, E. Forgoston, I. B. Schwartz, and P. A. Yecko, "Small and Adrift with Self-Control: Using the Environment to Improve Autonomy," in *: Bicchi A., Burgard W. (eds) Robotics Research*, vol. 3, pp. 387–402, Springer, Cham, 2018.

[3] D. Kularatne, S. Bhattacharya, and M. A. Hsieh, "Going with the flow: a graph based approach to optimal path planning in general flows," *Autonomous Robots*, vol. 42, no. 7, pp. 1369–1387, 2018.

[4] K. Y. Cadmus To, J. Ju Heon Lee, C. Yoo, S. Anstee, and R. Fitch, "Streamline-Based Control of Underwater Gliders in 3D Environments," in *Proceedings of the IEEE Conference on Decision and Control*, pp. 8303–8310, 2020.

[5] K. Y. C. To, K. M. B. Lee, C. Yoo, S. Anstee, and R. Fitch, "Streamlines for motion planning in underwater currents," in *Proceedings of the International Conference on Robotics and Automation*, pp. 4619–4625, 2019.

[6] J. Jouffroy and O. Zielinski, "On Active Current Selection for Lagrangian Profilers," *Identification and Control*, vol. 34, no. 1, pp. 1–10, 2013.

[7] S. Kemna, D. A. Caron, and G. S. Sukhatme, "Constraint-induced formation switching for adaptive environmental sampling," in *Proceedings of the MTS/IEEE OCEANS 2015*, pp. 1–7, 2015.

[8] M. Meghjani, F. Shkurti, J. C. G. Higuera, A. Kalmbach, D. Whitney, and G. Dudek, "Asymmetric rendezvous search at sea," in *Proceedings of the Canadian Conference on Computer and Robot Vision*, pp. 175–180, 2014.

[9] S. S. Kia, B. Van Scoy, J. Cortes, R. A. Freeman, K. M. Lynch, and S. Martinez, "Tutorial on dynamic average consensus: The problem, its applications, and the algorithms," *IEEE Control Systems Magazine*, vol. 39, no. 3, pp. 40–72, 2019.

[10] R. M. Murray, "Recent Research in Cooperative Control of Multivehicle Systems," *Journal of Dynamic Systems, Measurement, and Control*, vol. 129, no. 5, p. 571, 2007.

[11] A. Molchanov, A. Breitenmoser, S. Subbaraya, and G. Sukhatme, "Active Drifters : Sailing with the Ocean Currents," in *RSS Workshop on Autonomous Control, Adaptation, and Learning for Underwater Vehicles*, 2014.

[12] A. Valada, P. Velagapudi, B. Kannan, C. Tomaszewski, G. Kantor, and P. Scerri, "Development of a low cost multi-robot autonomous marine surface platform," in *Yoshida K., Tadokoro S. (eds) Field and Service Robotics. Springer Tracts in Advanced Robotics*, vol. 92, pp. 643–658, Springer, Berlin, Heidelberg, 2014.

[13] Z. Song, D. Lipinski, and K. Mohseni, "Multi-vehicle cooperation and nearly fuel-optimal flock guidance in strong background flows," *Ocean Engineering*, vol. 141, pp. 388–404, 2017.

[14] J. Moulton, N. Karapetyan, M. Kalaitzakis, A. Q. Li, N. Vitzilaios, and I. Rekleitis, "Dynamic Autonomous Surface Vehicle Controls Under Changing Environmental Forces," *arXiv preprint arXiv:1908.02850*, 2019.

[15] C. Tomlin, G. J. Pappas, and S. Sastry, "Conflict resolution for Air Traffic Management: A study in multiagent hybrid systems," *IEEE Transactions on Automatic Control*, vol. 43, no. 4, pp. 509–521, 1998.

[16] J. Das, F. Py, T. Maughan, T. O'Reilly, M. Messié, J. Ryan, G. S. Sukhatme, and K. Rajan, "Coordinated sampling of dynamic oceanographic features with underwater vehicles and drifters," *The International Journal of Robotics Research*, vol. 31, no. 5, pp. 626–646, 2012.

[17] V. Yordanova and H. Griffiths, "Synchronous rendezvous technique for multi-vehicle mine countermeasure operations," in *Proceedings of the MTS/IEEE OCEANS 2015*, pp. 1–6, 2015.

[18] A. Collins, J. Czyzowicz, L. Gasieniec, A. Kosowski, and R. Martin, "Synchronous rendezvous for location-aware agents," in *Peleg D. (eds) Distributed Computing. DISC 2011. Lecture Notes in Computer Science*, vol. 6950, pp. 447–459, Springer.

[19] M. M. Zavlanos, "Synchronous rendezvous of very-low-range wireless agents," in *Proceedings of the IEEE Conference on Decision and Control*, pp. 4740–4745, 2010.

[20] M. Michini, M. A. Hsieh, E. Forgoston, and I. B. Schwartz, "Robotic Tracking of Coherent Structures in Flows," *IEEE Transactions on Robotics*, vol. 30, no. 3, pp. 593–603, 2014.

[21] D. J. Larkin, "An Experimental Testbed for Creating Controlled Lagrangian Coherent Structures," Master's thesis, Drexel Univerisity, 2015.

[22] J. Marshall and R. A. Plumb, *Atmosphere, Ocean and Climate Dynamics: An Introductory Text (International Geophysics)*. Elsevier Academic Press, 2007.

[23] C. Wei, C. Li, and H. G. Tanner, "Synchronous Rendezvous for Periodically Orbiting Vehicles with Very-Low-Range Interactions," in *Proceedings of the IEEE American Control Conference*, pp. 1641–1646, 2018.

[24] C. Wei, X. Yu, H. G. Tanner, and M. A. Hsieh, "Synchronous Rendezvous for Networks of Active Drifters in Gyre Flows," in *Distributed Autonomous Robotic Systems* (Correll N., Schwager M., and Otte M, eds.), vol. 9, pp. 413–425, Springer, Cham, 2019.

[25] X. Yu, M. A. Hsieh, C. Wei, and H. G. Tanner, "Synchronous Rendezvous for Networks of Marine Robots in Large Scale Ocean Monitoring," *Frontiers in Robotics and AI*, vol. 6, p. 76, 2019.

[26] C. Wei, H. G. Tanner, X. Yu, and M. A. Hsieh, "Low-Range Interaction Periodic Rendezvous Along Lagrangian Coherent Structures," in *Proceedings of the IEEE American Control Conference*, pp. 4012–4017, 2019.

[27] C. Wei, H. G. Tanner, and M. A. Hsieh, "Nonlinear synchronization control for short-range mobile sensors drifting in geophysical flows," in *Proceedings of the IEEE International Conference on Robotics and Automation*, 2020. (to appear).

[28] A. Pikovsky, M. Rosenblum, J. Kurths, and R. C. Hilborn, "Synchronization: A Universal Concept in Nonlinear Science," *American Journal of Physics*, vol. 70, no. 6, pp. 655–655, 2002.

[29] E. M. Izhikevich, *Dynamical systems in neuroscience : the geometry of excitability and bursting*. MIT Press, 2007.

[30] E. Nozari and J. Cortés, "Oscillations and coupling in interconnections of two-dimensional brain networks," in *Proceedings of the IEEE American Control Conference*, pp. 193–198, 2019.

[31] M. Tyloo and P. Jacquod, "Global Robustness vs. Local Vulnerabilities in Complex Synchronous Networks," *Physical Review E*, vol. 100, no. 3, 2019.

[32] A. Jadbabaie, N. Motee, and M. Barahona, "On the Stability of the Kuramoto Model of Coupled Nonlinear Oscillators," in *Proceedings of the IEEE American Control Conference*, pp. 4296–4301, 2004.

[33] W. Ren and R. W. Beard, "Consensus of information under dynamically changing interaction topologies," in *Proceedings of the American Control Conference*, vol. 6, pp. 4939–4944, 2004.

[34] W. Ren, R. W. Beard, and T. W. McLain, "Coordination Variables and Consensus Building in Multiple Vehicle Systems," *In: Kumar V., Leonard N., Morse A.S. (eds) Cooperative Control. Lecture Notes in Control and Information Sciences*, vol. 309, pp. 171–188, 2005.

[35] M. Guo and M. M. Zavlanos, "Multirobot Data Gathering under Buffer Constraints and Intermittent Communication," *IEEE Transactions on Robotics*, vol. 34, no. 4, pp. 1082–1097, 2018.

[36] G. Hollinger and S. Singh, "Multi-robot coordination with periodic connectivity," in *Proceedings of the IEEE International Conference on Robotics and Automation*, pp. 4457–4462, 2010.

[37] Y. Qin, Y. Kawano, and M. Cao, "Stability of Remote Synchronization in Star Networks of Kuramoto Oscillators," in *Proceedings of the IEEE Conference on Decision and Control*, pp. 5209–5214, 2018.

[38] J. Sun, J. Liu, Y. Wang, Y. Yu, and C. Sun, "Fixed-time event-triggered synchronization of a multilayer Kuramoto-oscillator network," *Neurocomputing*, vol. 379, pp. 214–226, 2020.

[39] M. Ouimet and J. Cortes, "Coordinated rendezvous of underwater drifters in ocean internal waves," in *Proceedings of the IEEE Conference on Decision and Control*, pp. 6099–6104, 2014.

[40] H. G. Tanner, G. J. Pappas, and V. Kumar, "Leader-to-formation stability," *IEEE Transactions on Robotics and Automation*, vol. 20, no. 3, pp. 433–455, 2004.

[41] M. M. Zavlanos, H. G. Tanner, A. Jadbabaie, and G. J. Pappas, "Hybrid control for connectivity preserving flocking," *IEEE Transactions on Automatic Control*, vol. 54, no. 12, pp. 2869–2875, 2009.

[42] W. Mei and F. Bullo, "LaSalle Invariance Principle for Discrete-time Dynamical Systems: A Concise and Self-contained Tutorial," *http://arxiv.org/abs/1710.03710*, 2017.

[43] D. Kularatne, S. Bhattacharya, and M. Ani Hsieh, "Time and Energy Optimal Path Planning in General Flows," in *Robotics: Science and Systems XII*, 2016.

[44] H. K. Khalil, *Nonlinear systems*. Prentice Hall, 2002.